9 ATMOSPHERIC CHEMISTRY

Early air pollution studies dealt with the challenging problem of correctly simulating atmospheric diffusion and, in particular, the maximum ground-level impact of elevated emissions of primary pollutants, such as SO_2. Two major factors, however, focused attention on atmospheric chemistry: 1) photochemical smog, a new, different smog associated with high-temperature "summertime" conditions, and first recognized in the Los Angeles basin in the 1940s; and 2) long-range transport phenomena, clearly identified in the 1970s, that led to the study of multiday transport scenarios of industrial and urban plumes and, consequently, to the simulation of the formation, inside them, of secondary gases and particles.

Atmospheric chemistry deals essentially with four major issues (Seigneur, 1987):

1. Photochemical smog in sunny, urban areas, such as Los Angeles and Mexico City
2. Aerosol chemistry
3. Acidic deposition by dry and wet deposition phenomena (see Section 10)
4. Air toxics

In addition to the above topics, fog chemistry plays an important role, even though understanding of it is limited at the present time.

A correct treatment of atmospheric chemistry requires the solution of chemical kinetic and thermodynamic equations and, when necessary, some treatment of those physical processes (e.g., cloud microphysics, aerosol size, etc.) that affect the evolution of the chemistry of the system. A complete discussion of chemical processes in the atmosphere is beyond the scope of this book. The reader is referred to Seinfeld (1986) and Finlayson-Pitts and Pitts (1986) for a thorough discussion of this subject. In this chapter, we will provide a summary of the major issues related to the understanding and computer simulation of the major atmospheric chemistry phenomena.

9.1 PHOTOCHEMICAL SMOG: NITROGEN OXIDES AND OZONE

Ozone is the major indicator of the presence of urban photochemical smog. Ozone is naturally generated in the stratosphere by a photochemical reaction in which high-energy solar radiation breaks the oxygen molecules, i.e.

$$O_2 + h\nu\ (\lambda < 242\ \text{nm}) \rightarrow 2\,O\cdot \tag{9-1}$$

The oxygen atoms then combine with oxygen molecules to form ozone, i.e.

$$O\cdot + O_2 \rightarrow O_3 \tag{9-2}$$

A small fraction of this stratospheric layer of ozone penetrates the PBL and is responsible for the ambient background concentration of O_3. Stratospheric ozone intrusion into the PBL is also responsible for some natural high concentration values, following large convective thunderstorms.

Anthropogenic generation of O_3 is, again, a photochemical process, in which NO_2, mostly generated from emissions of primary NO from combustion processes, is photochemically dissociated by

$$NO_2 + h\nu\ (\lambda < 430\ \text{nm}) \rightarrow NO + O\cdot \tag{9-3}$$

and the oxygen atom produces ozone via Equation 9-2. This chemical mechanism is the only known process for ozone formation in a polluted atmosphere.

Ozone is scavenged by its reaction with combustion emissions of NO

$$NO + O_3 \rightarrow NO_2 + O_2 \tag{9-4}$$

This reaction is highly effective at night inside the mixing layer because, without solar radiation, the NO_2 cannot be further dissociated by Equation 9-3. Above the mixing layer, however, ozone is not consumed and may, therefore, be fumigated to the ground the following morning, when the nighttime ground-level inversion breaks.

Because of the reaction scheme described above, it is evident that any reaction converting NO to NO_2 (besides Equation 9-4, which actually reduces O_3 concentrations) contributes to ozone formation. NO_2 is formed in combustion exhaust gases by

$$2NO + O_2 \rightarrow 2NO_2 \qquad (9\text{–}5)$$

However, it can be easily seen (e.g., Seinfeld, 1986) that Equation 9–5 is insufficient to account for the O_3 concentrations of a few hundred pbb that are commonly measured during urban photochemical episodes. It has been well established that the NO-to-NO_2 conversion, in a polluted atmosphere, is dominated by the carbon-containing species, as discussed in the next section.

9.2 PHOTOCHEMICAL SMOG: THE ROLE OF THE CARBON-CONTAINING SPECIES

The role of carbon-containing species is essential to understand the NO-to-NO_2 conversion and, consequently, the occurrence of high ozone concentrations.

The simplest carbon-containing species is CO, whose reaction with NO_x is summarized in Table 9–1. This reaction scheme indicates that ozone photolyzes (Reaction 4) to produce an excited $O(^1D)$ oxygen atom, which collides with water (Reaction 6) to produce the two hydroxyl radicals $OH\cdot$, that react with the carbon monoxide (Reaction 7) to produce the hydroperoxyl radical $HO_2\cdot$, a species that is responsible for the oxidation of NO into NO_2 (Reaction 8). Note that the other

Table 9–1. Atmospheric chemistry of CO and NO_x (from Seinfeld, 1986). [Reprinted with permission from John Wiley and Sons.]

Reaction	Rate Constant[a]
1. $NO_2 + h\nu \rightarrow NO + O$	Depends on light intensity
2. $O + O_2 + M \rightarrow O_3 + M$	$6.0 \times 10^{-34}(T/300)^{-2.3}$ cm^6 molecule^{-2} sec^{-1}
3. $O_3 + NO \rightarrow NO_2 + O_2$	$2.2 \times 10^{-12}\exp(-1430/T)$ cm^3 molecule^{-1} sec^{-1}
4. $O_3 + h\nu \rightarrow O(^1D) + O_2$	$0.0028k_1$
5. $O(^1D) + M \rightarrow O + M$	2.9×10^{-11} cm^3 molecule^{-1} sec^{-1}
6. $O(^1D) + H_2O \rightarrow 2OH\cdot$	2.2×10^{-10} cm^3 molecule^{-1} sec^{-1}
7. $CO + OH\cdot \rightarrow CO_2 + HO_2\cdot$	2.2×10^{-13} cm^3 molecule^{-1} sec^{-1}[b]
8. $HO_2\cdot + NO \rightarrow NO_2 + OH\cdot$	$3.7 \times 10^{-12}\exp(240/T)$ cm^3 molecule^{-1} sec^{-1}
9. $OH\cdot + NO_2 \rightarrow HNO_3$	1.1×10^{-11} cm^3 molecule^{-1} sec^{-1}

[a] Baulch et al. (1982).
[b] Atkinson and Lloyd (1984).

radical, $OH\cdot$, is also responsible for the formation of nitric acid HNO_3, through its reaction with NO_2 (Reaction 9).

A similar cycle can be identified for formaldehyde *HCHO*, which is both emitted as primary pollutant and generated as an oxidation product of hydrocarbons. The *HCHO* cycle is presented in Table 9–2. In this cycle, formaldehyde, either by photodissociation (Reaction 4a) or reaction with $OH\cdot$ (Reaction 5), produces the radical $HO_2\cdot$, which oxidizes *NO* into NO_2 (Reaction 6). Figure 9–1 shows how the formation of NO_2 (and, therefore, O_3) is driven by the initial concentration of *HCHO*. Clearly, many other hydrocarbons are involved, but the major features of photochemical smog chemistry are well exemplified by this $NO_x/HCHO$ mechanism.

Other hydrocarbons, besides formaldehyde, include other aldehydes, ketones, paraffins (i.e., alkanes), olefins (i.e., alkenes) and aromatics. Table 9–3 summarizes the typical lifetimes of these hydrocarbons in a polluted atmosphere.

9.3 PHOTOCHEMICAL SMOG: SIMULATION MODELING

Mathematical modeling of photochemical smog requires the numerical simulation of all the chemical reactions that take place between NO_x and

Table 9–2. Atmospheric reaction mechanism involving NO, NO_2 and HCHO (from Seinfeld, 1986). [Reprinted with permission from John Wiley and Sons.]

Reaction	Rate Constant
1. $NO_2 + h\nu \rightarrow NO + O$	Depends on light intensity
2. $O + O_2 + M \rightarrow O_3 + M$	See Table 9–1
3. $O_3 + NO \rightarrow NO_2 + O_2$	See Table 9–1
4. $HCHO + h\nu \rightarrow 2HO_2\cdot + CO$	Depends on light intensity
$\rightarrow H_2 + CO$	Depends on light intensity
5. $HCHO + OH\cdot \rightarrow HO_2\cdot + CO + H_2O$	1.1×10^{-11} cm^3 molecule^{-1} sec^{-1} [a]
6. $HO_2\cdot + NO \rightarrow NO_2 + OH\cdot$	See Table 9–1
7. $OH\cdot + NO_2 \rightarrow HNO_3$	See Table 9–1

[a] Baulch et al. (1982)

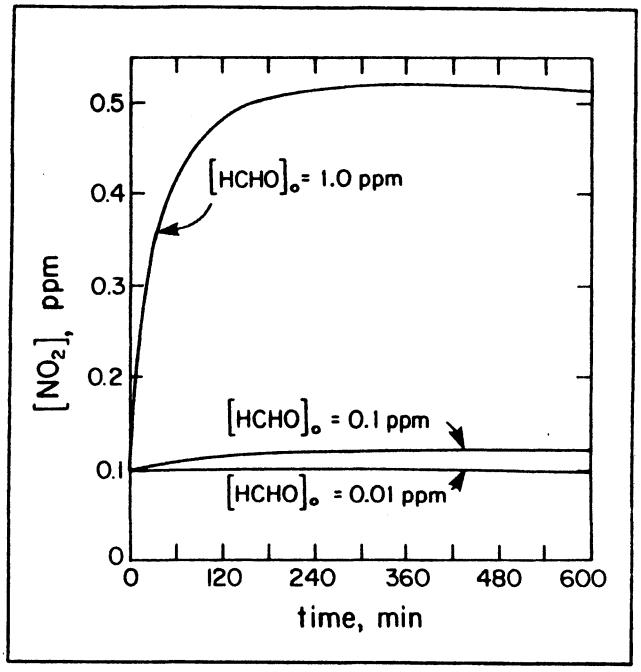

Figure 9–1. Effect of initial concentration of formaldehyde on the dynamics of NO_2 in the photooxidation of a mixture of HCHO, NO, and NO_2 in the air. In the three cases shown, $[NO_2]_0 = 0.1$ ppm and $[NO]_0 = 1.0$ ppm (from Seinfeld, 1986). [Reprinted with permission from John Wiley and Sons.]

carbon-containing compounds, such as paraffins, olefins, aldeydes, ketones and aromatic compounds. An explicit treatment of all these reactions is practically impossible. For example, Kerr and Calvert (1984) developed a chemical kinetic mechanism that includes over 1,000 chemical reactions. Clearly, for most practical purposes, the numerical simulations must use a condensed kinetic mechanism to avoid excessive simulation costs (a portion of an explicit chemical mechanism is presented in Table 9–4).

Three major approaches have been taken (Seigneur, 1987) to develop condensed and computationally affordable kinetic mechanisms for modeling:

1. Surrogate species mechanisms, in which a few hydrocarbons are selected as representative of their respective hydrocarbon class

2. Lumped molecule mechanisms, in which hydrocarbons from the same class are lumped together and a hypothetical species is defined to represent each class (a portion of a lumped mechanism is presented in Table 9–5)

Table 9–3. Photolysis and oxidation lifetime of hydrocarbons in a typical polluted atmosphere[a] (from Seigneur, 1987). [Reprinted with permission from Computational Mechanics Publications.]

Hydrocarbon	Photolysis	O_3 Reaction	OH Reaction	O Reaction	HO_2 Reaction	NO_3 Reaction
Formaldehyde	2 h	--	6 h	--	4 h	8 d
Other Aldehydes	6 h	--	2 to 5 h	--	--	2 to 4 d
Ketones		--	2 h to 10 d	--	--	(b)
Methane	--	--	9 mo	--	--	--
Other Paraffins	--	--	10 min to 9 d	--	--	20 d to 8 mo
Anthropogenic Olefins	--	5 min to 2 d	50 min to 7 h	3 d to 1 y	--	8 s to 3 mo
Natural Olefins	--	1 to 7 h	30 min to 1 h	(b)	--	40 s to 20 min
Alkynes	--	--	7 h to 3 d	--	--	--
Aromatics (nonoxygenated)	--	--	2 h to 2 d	--	--	18 d to 8 mo
Aromatics (oxygenated)	--	--	1 to 2 h	--	--	10 to 30 s

(a) Conditions are for summertime, concentrations of 120 ppb of O_3, 0.2 ppt of OH, 0.002 ppt of O, 40 ppt of HO_2 and 100 ppt of NO_3. Photolysis and reactions with O_3, OH, O and HO_2 are important during daytime, reactions with NO_3 are important at night. Lifetimes which exceed 1 year are not listed. The lifetime is defined as the inverse of the first-order or pseudo-first-order reaction rate parameter. Therefore, it corresponds to the time necessary for the hydrocarbon concentration to decrease to 37 percent of its initial value.
(b) Not available.

3. Carbon-bond mechanism, in which the classification is based on chemical bonds of hydrocarbons and their reactivity (a portion of the carbon-bond mechanism is presented in Table 9–6)

Simulation models based on the above mechanisms are applied, with the major goal of quantifying the complex, nonlinear relationship between the emissions of primary precursors (i.e., NO_x and volatile organic compounds, VOC, often referred to as reactive hydrocarbons, RHC, or nonmethane hydrocarbons, NMHC) and the maximum ground level concentrations of O_3. It is still a major technical and political challenge, in regions like the Los Angeles basin, to assess, in a proper and technically credible way, the most cost-effective reduction of NO_x and VOC emissions that will give a desired decrease in O_3 concentrations

Table 9–4. Portion of an explicit chemical mechanism (from Finlayson–Pitts and Pitts, 1986). [Reprinted with permission from John Wiley and Sons.]

Reaction	Rate Constant[a]
Inorganic Reactions	
(1) $NO_2 + h\nu \rightarrow NO + O(^3P)$	0.35–0.40 min^{-1}
(2) $O(^3P) + O_2 \rightarrow O_3$	2.6×10^1
(3) $O_3 + NO \rightarrow NO_2 + O_2$	2.7×10^1
(4) $O(^3P) + NO_2 \rightarrow NO + O_2$	1.4×10^4
(5) $O_3 + NO_2 \rightarrow NO_3 + O_2$	4.7×10^{-2}
etc.	
Aldehyde Reactions and PAN Formation	
(30) $CH_3CHO + h\nu \xrightarrow{2O_2} CH_3O_2 + HO_2 + CO$	*b*
(31) $CH_3CHO + OH \xrightarrow{O_2} CH_3CO_3 + H_2O$	2.4×10^4
(32) $CH_3O_2 + NO \rightarrow NO_2 + CH_3O$	1.1×10^4
etc.	
α-Dicarbonyl Chemistry	
(43) $CH_3COCHO + OH \xrightarrow{O_2} CH_3COO_2 + CO + H_2O$	2.5×10^4
(44) $CH_3COCHO + h\nu \xrightarrow{2O_2} CH_3COO_2 + HO_2 + CO$	*c*
(45) $CH_3COCHO + h\nu \xrightarrow{2O_2} CH_3O_2 + HO_2 + 2CO$	*c*
etc.	
Toluene Abstraction Pathway	
(48) $C_6H_5CH_3 + OH \xrightarrow{O_2} C_6H_5CH_2O_2 + H_2O$	7.5×10^2
(49) $C_6H_5CH_2O_2 + NO \xrightarrow{O_2} NO_2 + C_6H_5CHO$	9.0×10^3
(50) $C_6H_5CH_2O_2 + NO \rightarrow C_6H_5CH_2ONO_2$	1.0×10^3
etc.	
Toluene Addition Pathway	
(64) $C_6H_5CH_3 + OH \rightarrow C_6H_5(CH_3)OH$	8.7×10^3
(65) $C_6H_5(CH_3)OH + O_2 \rightarrow C_6H_4(CH_3)OH + HO_2$	1.0×10^1
(66) $C_6H_5(CH_3)OH + NO_2 \rightarrow C_6H_4(CH_3)NO_2 + H_2O$	4.4×10^4
etc.	
Conjugated α-Dicarbonyl Chemistry	
(82) $OHCCH{=}CHCHO + OH \xrightarrow{O_2} OHCCH{=}CHC(O)O_2 + H_2O$	4.4×10^4
(83) $OHCCH{=}CHC(O)O_2 + NO \xrightarrow{O_2} OHCCH{=}CHO_2 + NO_2 + CO_2$	1.0×10^4
etc.	

Source: Leone and Seinfeld, 1984.

[a] In units of $ppm^{-1}\ min^{-1}$ unless otherwise stated.

[b] $k_{30} = 8.4 \times 10^{-4}\ k_1$.

[c] $(k_{44} + k_{45}) = 0.019\ k_1$.

Table 9–5. Portion of a lumped chemical submodel used for modeling an urban airshed (from Finlayson–Pitts and Pitts, 1986). An updated version of this mechanism is found in Lurmann et al. (1985). [Reprinted with permission from John Wiley and Sons.]

Reaction	Rate Constant[a]
(1) $NO_2 + h\nu \rightarrow NO + O(^3P)$	0.339 min^{-1}[b]
(2) $O(^3P) + O_2 + M \rightarrow O_3 + M$	$3.9 \times 10^{-6}\, e^{510/T}$
⋮	⋮
(21) $HCHO + h\nu \rightarrow 2HO_2 + CO$	0.00163 min^{-1}
(22) $HCHO + h\nu \rightarrow H_2 + CO$	0.00296 min^{-1}
(23) $HCHO + OH \rightarrow HO_2 + H_2O + CO$	1.9×10^4
(24) $RCHO + h\nu \rightarrow RO_2 + HO_2 + CO$	0.00145
(25) $RCHO + OH \rightarrow RCO_3$	2.6×10^4
(26) $C_2H_4 + OH \rightarrow RO_2$	1.2×10^4
(27) $C_2H_4 + O \rightarrow RO_2 + HO_2$	1.2×10^3
(28) $OLE + OH \rightarrow RO_2$	8.9×10^4
(29) $OLE + O \rightarrow RO_2 + RCO_3$	2.2×10^4
(30) $OLE + O_3 \rightarrow (a_1)RCHO + (a_2)HCHO + (a_3)HO_2 + (a_4)RO_2 + (a_5)OH + (a_6)RO$	0.136
(31) $ALK + OH \rightarrow RO_2$	4.7×10^3
(32) $ALK + O \rightarrow RO_2 + OH$	99.8
(33) $ARO + OH \rightarrow RO_2 + RCHO$	1.6×10^4
(16) $RO_2 + NO \rightarrow RO + NO_2$	1.2×10^4
(18) $NO_2 + OH \rightarrow HNO_3$	1.5×10^4
(42) $RCO_3 + NO_2 \rightarrow PAN$	2.07×10^3
(43) $PAN \rightarrow RCO_3 + NO_2$	$4.77 \times 10^{16}\, e^{-12516/T}$
(44) $NO_2 + NO_3 \rightarrow N_2O_5$	$2.19 \times 10^2\, e^{861/T}$
(46) $N_2O_5 + H_2O \rightarrow 2HNO_3$	1.5×10^{-5}
⋮	⋮
(52) $2RO_2 \rightarrow 2RO$	196

Source: McRae et al., 1982a,b.

[a] In units of ppm^{-1} min^{-1} unless otherwise stated.

[b] Average of daylight hours.

to meet the local air quality standards. These are the type of multibillion dollar air quality control questions that can properly be answered only through the application of the most advanced photochemical models.

Several Lagrangian and Eulerian models contain numerical routines for the treatment of multispecies chemical reactions. A description of the practical implementation of a photochemical reaction mechanism (i.e., a numerical

simulation scheme) in an Eulerian grid model is described by McRae et al. (1982b) and briefly summarized below. Also, particularly important is the "Atkinson–Carter" gas-phase photochemical mechanism, which has been implemented into a flexible, easy-to-update software system (Carter, 1988). This mechanism can run in its most complete version, can be extended to include new representations, can be refined by the choice of parameters, and, finally, can be condensed for practical use in airshed models. Appropriate software tools make the above operations much easier to perform than with other mechanisms.

Table 9–6. A portion of the carbon bond mechanism (from Finlayson–Pitts and Pitts, 1986). An updated version of this mechanism can be found in Gery et al. (1987). [Reprinted with permission from John Wiley and Sons.]

Reaction	Rate Constant ($ppm^{-1}\ min^{-1}$)
$NO_2 + h\nu \rightarrow NO + O$	k_1[a]
$O + O_2 (+ M) \rightarrow O_3 (+ M)$	2.08×10^{-5}
$O_3 + NO \rightarrow NO_2 + O_2$	25.2
$O + NO_2 \rightarrow NO + O_2$	1.34×10^{4}
$O_3 + NO_2 \rightarrow NO_3 + O_2$	5×10^{-2}
$NO_3 + NO \rightarrow NO_2 + NO_2$	2.5×10^{4}
$NO_3 + NO_2 + H_2O \rightarrow 2HNO_3$	2.0×10^{-3}
$HNO_2 + h\nu \rightarrow NO + OH$	$0.19\ k_1$
$NO_2 + OH \rightarrow HNO_3$	1.4×10^{4}
$NO + OH \rightarrow HNO_2$	1.4×10^{4}
$CO + OH \xrightarrow{O_2} CO_2 + HO_2$	4.5×10^{2}
$OLE + OH \xrightarrow{O_2} CAR + CH_3O_2$	3.8×10^{4}
$PAR + OH \xrightarrow{O_2} CH_3O_2 + H_2O$	1.3×10^{3}
$ARO + OH \xrightarrow{O_2} CAR + CH_3O_2$	8×10^{3}
$OLE + O \xrightarrow{2O_2} HC(O)O_2 + CH_3O_2$	5.3×10^{3}
$PAR + O \xrightarrow{O_2} CH_3O_2 + OH$	20
$ARO + O \xrightarrow{2O_2} HC(O)O_2 + CH_3O_2$	37
$ARO + NO_3 \rightarrow$ products (aerosol)	1.0×10^{2}
$OLE + O_3 \xrightarrow{O_2} \alpha[HC(O)O_2] + HCHO + OH$	1.5×10^{-2}
$CAR + OH \xrightarrow{O_2} HC(O)O_2 + H_2O$	1.0×10^{4}
$CAR + h\nu \xrightarrow{2O_2} \alpha HC(O)O_2 + \alpha HO_2 + (1 - \alpha)CO$	$6.0 \times 10^{-3}\ k_1$

Source: Whitten and Hogo, 1977; Whitten et al., 1980.
[a]Varies with light intensity.

9.3.1 A Numerical Simulation Scheme

Using the approximation of Equation 6–15, chemical reactions are represented by the terms R_{c_m}, $m = 1, 2 \ldots M$. If we assume a homogeneous, isothermal, isobaric system with M single-phase species ($m = 1, 2, \ldots M$), which simultaneously participate in N elementary reaction steps ($n = 1, 2, \ldots N$), then, formally, the reaction set can be written in terms of linear combinations

$$\sum_{m=1}^{M} r_{nm}\, c_m \rightarrow \sum_{m=1}^{M} p_{nm}\, c_m \; ; \; n = 1, 2, \ldots N \tag{9–6}$$

This equation extends over all M species, to allow for the possibility that a given species can participate in a reaction as both a product and a reactant.

Equation 9–6 can be written in a compact matrix notation

$$\mathbf{Rc} \rightarrow \mathbf{Pc} \tag{9–7}$$

where $\mathbf{c}$ is the concentration $\mathbf{c} = [c_1, c_2, \ldots c_m]^T$, and $\mathbf{R}$ and $\mathbf{P}$ are the reactant and product stoichiometric matrices, respectively, which contain the $N \times M$ elements r_{nm} and p_{nm}. If the rates f_n of the N individual reactions are given, then the kinetics of the reaction set is described by the following set of ordinary differential equations

$$d\mathbf{c}/dt = \mathbf{S}^T \mathbf{F} \tag{9–8}$$

where $\mathbf{S}$ is the stoichiometric matrix

$$\mathbf{S} = \mathbf{P} - \mathbf{R} \tag{9–9}$$

and $\mathbf{F} = [f_1, f_2, \ldots f_N]^T$. Equation 9–8 can be numerically integrated if appropriate initial conditions are provided.

The determination of $\mathbf{F}$ is still a major area of experimental and theoretical investigation. For diluted chemical systems, a common approximation is the so-called "mass action law," in which f_n can be expressed as a product of the concentration c_m of the species involved in the n-th reaction, i.e.,

$$f_n = k_n \prod_{m=1}^{M} c_m^{r_{nm}} \tag{9–10}$$

where k_n is a temperature-dependent rate constant given by

$$k_n(T) = A_n \exp(-B_n/T) \tag{9-11}$$

Due to the large number of hydrocarbons, many chemical mechanisms use the "lumped" approach, in which hydrocarbon chemistry is given by

$$HC_j + X_y \xrightarrow{\overline{k}_j^{(y)}} \text{products} \tag{9-12}$$

which involves a reaction between the molecule X_y (typically atomic oxygen O, hydroxyl radical OH, or ozone O_3) and the j-th hydrocarbon class. It is assumed that all hydrocarbons are divided into reactivity classes, such as olefins, aromatics, alkanes and aldehydes. The computation of the "lumped" rate constants $\overline{k}_j^{(y)}$ is given by

$$\overline{k}_j^{(y)} = \frac{\sum_{p=1}^{p_j} k_p^{(y)} n_p}{\sum_{p=1}^{p_j} n_p} \tag{9-13}$$

where n_p is the number of moles of the generic species p in the hydrocarbon class j, and $k_p^{(y)}$ is the rate constant for the reaction rate between the species p and X_y.

Some key reactions in the photochemical models involve the photolysis of such species as nitrogen dioxide NO_2, formaldehyde $HCHO$, and nitrous acid $HONO$. For a typical species A, the photodissociation step can be written as

$$A + h\nu \xrightarrow{k} \text{products} \tag{9-14}$$

with the forward reaction rate

$$R = -dc_A/dt = k\, c_A \tag{9-15}$$

where c_A is the concentration of the species A.

The photolysis rate constant k, at the spatial location $\mathbf{x}$ and time t, of any pollutant present in the atmosphere in small concentrations is given by the numerical integration of

$$k = \int_0^\infty \sigma\,[\lambda,\ T(\mathbf{x})]\ \phi\,[\lambda,\ T(\mathbf{x})]\ I\,[\lambda,\ t,\ \mathbf{x}]\ d\lambda \qquad (9\text{-}16)$$

where $\sigma\,[\lambda, T(\mathbf{x})]$ is the wavelength (λ) dependent absorption cross section (cm^2) for the species at temperature $T(\mathbf{x})$; $\phi\,[\lambda, T(\mathbf{x})]$ is the quantum yield for the reaction; and I is the actinic irradiance (photons/cm^2-sec). The numerical evaluation of Equation 9-16 requires data for the species absorption cross sections and quantum yields as a function of λ and the local zenith angle.

9.3.2 Eulerian and Lagrangian Implementations

Photochemical schemes, such as those presented above, are able to calculate the dynamics of all photochemical species in each computational cell at each time step. In Eulerian photochemical models (e.g., McRae et al., 1982b, Tesche et al., 1984, and Carmichael et at., 1986) the K-theory is used to simulate atmospheric diffusion and a three-dimensional grid is superimposed to cover the entire computational domain. (Efforts were also made to embed one or more reactive plume models into K-theory grid models, as in the Plume-Airshed Reactive-Interactive System (PARIS) developed by Seigneur et al., 1983.) In the Lagrangian photochemical models (e.g., API, 1985; Lurmann et al., 1985), which were discussed in Section 8.2, columns or walls of cells are advected according to the main wind, in a way that allows the incorporation of the emissions encountered along their trajectory. Lagrangian models also use K-theory to calculate vertical and (when available) horizontal diffusion.

The main advantage of Lagrangian models versus Eulerian ones is computational speed, which can be one to two orders of magnitude faster because of the smaller number of grid cells used in Lagrangian models versus Eulerian models(*). Lagrangian models, however, provide concentration outputs along trajectories and, therefore, their outputs are difficult to compare with concentration measurements at fixed locations. Examples of simulations by photochemical Eulerian models are presented in Figures 9-2 and 9-3. It should be noted that the only photochemical model currently recommended (i.e., with a "preferred" status) by the U.S. EPA is the Urban Airshed Model (UAM), an Eulerian K-theory grid model that employs a simplified version of the Carbon-Bond II Mechanism (Ames et al., 1985a and 1985b). The UAM model is discussed in Section 14.1.1.

(*)The new generation of micro- and mini-computers, however, has sharply decreased computer costs. Today, an Eulerian photochemical model can perform a three-day simulation of a large air basin (such as Los Angeles) on a workstation in less than 16 CPU hours (Tesche, personal communication).

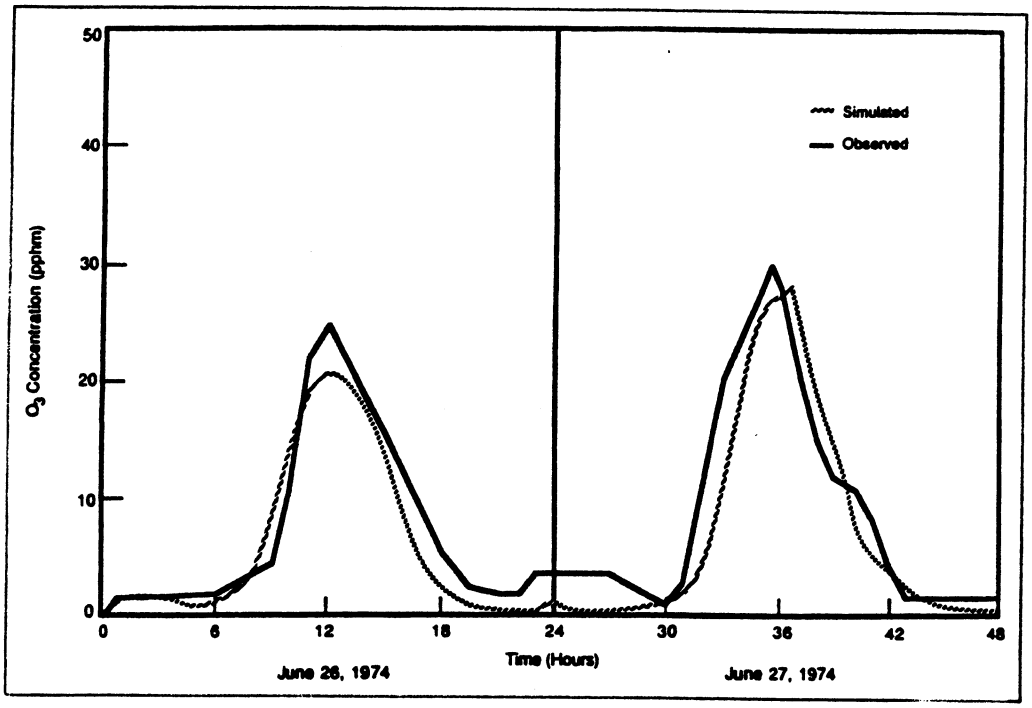

Figure 9–2. Simulation of the ozone concentration at the Pasadena monitoring station in the Los Angeles metropolitan area (from Seigneur, 1987). [Reprinted with permission from Computational Mechanics Publications.]

9.3.3 The EKMA Technique

A proper elaboration of the outputs of Lagrangian photochemical models allows the use of a simple method, the so-called EKMA (Empirical Kinetic Modeling Approach) technique (Dodge, 1977) to evaluate the importance of both NMHC and NO_x (and their ratio) in formulating O_3 control strategies. An example of EKMA isopleths is presented in Figure 9–4, in which point A illustrates a city that is characterized by an NMHC/NO_x ratio of 8:1 and a "design" value (defined as the second highest hourly O_3 measured concentration) of O_3 of 0.28 ppm. The isopleths allow the definition of different strategies to meet a certain ozone air quality standard. For example, if no change in ambient NO_x is expected and the future goal for the design value of ozone is 0.12 ppm, then the control strategy requires a progress from point A to point B in Figure 9–4, i.e., a reduction of NMHC by approximately 67 percent.

As seen in the example above, the EKMA method establishes, graphically, a relationship between the concentrations of ozone "precursors" (NO_x and NMHC) and the design value of ozone. Note the nonlinearities in Figure 9–4:

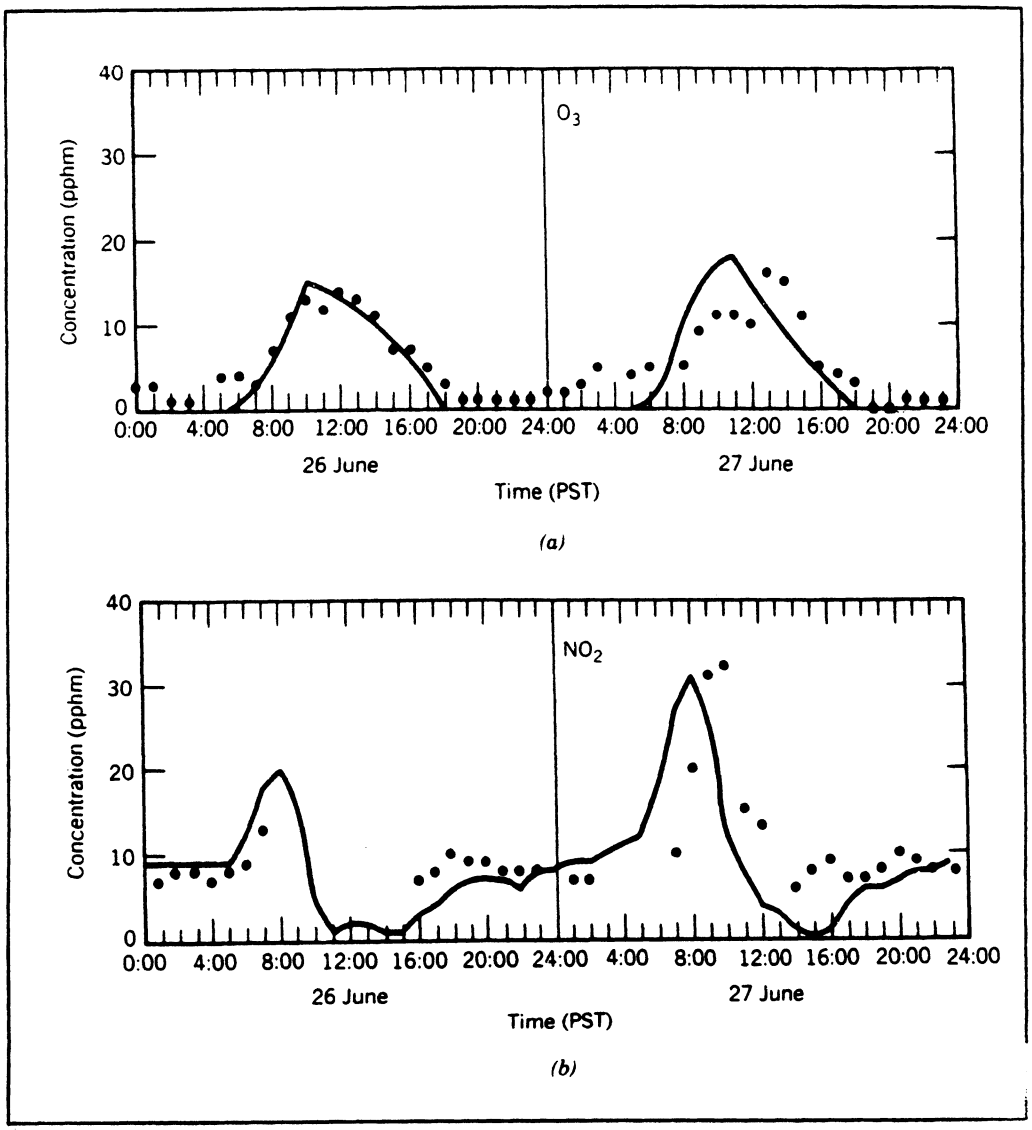

Figure 9–3. Observed (●) and model predicted (—) concentrations of (a) O_3 and (b) NO_2 in downtown Los Angeles, June 26 and 27, 1974 (from McRae and Seinfeld, 1983, as presented by Finlayson–Pitts and Pitts, 1986). [Reprinted with permission from John Wiley and Sons.]

depending on the position of A, different emission reductions of NMHC and/or NO_x can cause both decrease and *increase* of O_3. For example, for high NMHC/NO_x ratios, O_3 does not vary with NHMC controls, while for low NMHC/NO_x ratios, NO_x controls can actually *increase* O_3.

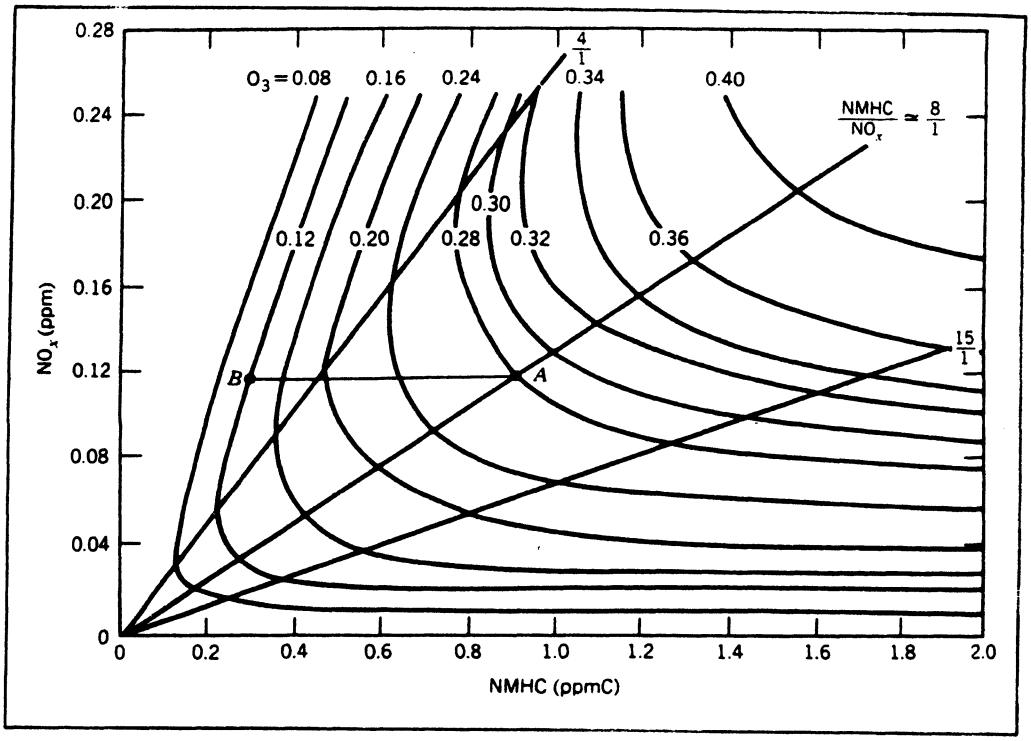

Figure 9–4. Ozone isopleths used in the EKMA approach (from Dodge, 1977, as presented by Finlayson–Pitts and Pitts, 1986). [Reprinted with permission from John Wiley and Sons.]

EKMA isopleths should be used with caution, since they represent an oversimplified empirical description of complex nonlinear phenomena. The generic isopleths in Figure 9–4 are based on a series of chemical, meteorological, geographical, background and emission assumptions. A computer program, the OZIPM–2 package (Gipson, 1984) allows the generation of city–specific isopleths, under conditions defined by the user.

9.4 AEROSOL CHEMISTRY

A detailed discussion of aerosol chemistry is clearly beyond the scope of this book. Therefore, in this section, we briefly discuss the major problems related to aerosol formation and dynamics. We also present a few recent modeling mechanisms.

Atmospheric aerosols consist of primary aerosol (i.e., directly emitted into the atmosphere; e.g., fugitive dust) and secondary aerosol, which is formed in the atmosphere through chemical reactions (e.g., sulfates). Typically (Seigneur, 1987), secondary aerosol range in size from about 0.01 μm to 2 μm, while primary aerosols are associated with larger sizes of about 1μm to 100 μm.

Aerosols play an important role in many air pollution studies. Small particles can be inhaled and cause adverse effects to the human pulmonary system. Also, particulate matter in the range of 0.1 to 1 μm is the most efficient at scattering light and, therefore, secondary aerosols are often the major cause of anthropogenic impairment of atmospheric visibility. Finally, sulfate and nitrate aerosols are the major cause of acidic deposition.

The formation of secondary particulate matter is due to several mechanisms (Finlayson-Pitts and Pitts, 1986):

1. reaction of gases to form low-vapor-pressure products, which combine to form new particles or condense on preexisting particles
2. reaction of gases on the surfaces of existing particles to form condensed products
3. chemical reactions within the aerosol itself

These mechanisms are illustrated in Figure 9-5.

The complex chemistry of secondary aerosols involves three phases (Seigneur, 1987):

1. the gas phase, where condensable species are chemically formed
2. the aerosol aqueous phase, where chemical reactions can take place
3. the aerosol solid phase, which may deliquence into aqueous phase, and vice versa.

A comprehensive discussion of gas-phase and aqueous-phase atmospheric chemistry is presented in Seinfeld (1986).

9.4.1 The SO_2 - to - SO_4^{2-} Formation

Secondary sulfates represent, in most cases, the major problem in aerosol acid precipitation and visibility studies. The formation of sulfates SO_4^{2-} from primary emissions of SO_2 follows the pattern described below (Seinfeld, 1986).

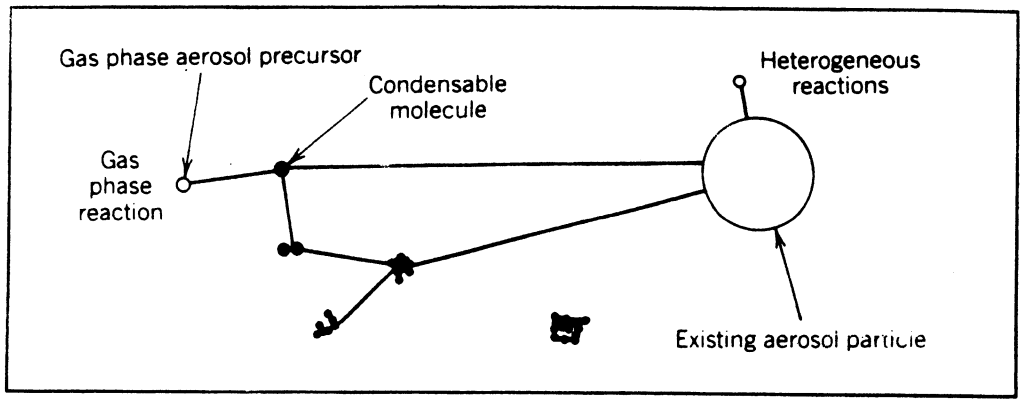

Figure 9–5. *A schematic diagram showing aerosol formation by different chemical mechanisms. Condensable molecules formed by chemical reactions involving gas-phase precursors can combine with other condensable molecules or molecular clusters to form new particles, or condense on preexisting aerosol causing them to grow. Alternatively, aerosol precursor gases can react to form a secondary aerosol on the surface of, or within, existing aerosol particles (from McMurry and Wilson, 1982, as presented by Finlayson–Pitts and Pitts, 1986). [Reprinted with permission from John Wiley and Sons.]*

Sulfur dioxide has a tendency to react with oxygen in air, thus giving

$$2SO_2 + O_2 \rightarrow 2SO_3 \qquad (9\text{–}17)$$

In a moist atmosphere, SO_3 reacts with water vapor to form sulfuric acid

$$SO_3 + H_2O \rightarrow H_2SO_4\ (aq) \qquad (9\text{–}18)$$

The above reactions, though thermodynamically favorable, are in general very slow and, therefore, are not important under most atmospheric conditions. When liquid-phase catalytic reactions of SO_2 are not important, gas reactions are mostly

$$OH\cdot + SO_2 \rightarrow HOSO_2\cdot \qquad (9\text{–}19)$$

which is probably followed by

$$HOSO_2\cdot + O_2 \rightarrow HO_2\cdot + SO_3 \tag{9-20}$$

$$SO_3 + H_2O \rightarrow H_2SO_4 \tag{9-21}$$

The reactions above describe the gas-phase oxidation of SO_2. An important role however, is often played by SO_2 oxidation inside fog or cloud droplets, which follows other reaction pathways.

Once H_2SO_4 is produced, it will rapidly acquire water vapor and nucleate to form small particles or condense on existing particles. If enough ammonia (NH_3) gas is present in the atmosphere, it will neutralize the acidic H_2SO_4, thus creating ammonium sulfate $(NH_4)_2SO_4$, the preferred form of sulfate, in condensed or particulate form. Otherwise, ammonium bisulfate NH_4HSO_4 or letovicite $(NH_4)_3\,H(SO_4)_2$ will be produced.

Experimental studies have shown that the complex homogeneous (i.e., gas-phase) SO_2-to-SO_4^{2-} conversion is strongly dependent upon ambient concentration values of the free radical $OH\cdot$; this allows the definition and use of semiempirical formulas for SO_2 oxidation, such as (SAI, 1984)

$$-\frac{1}{[SO_2]}\,\frac{d[SO_2]}{dt} = k_{22}\,[OH] \tag{9-22}$$

where the brackets indicate concentrations and $k_{22} \simeq 2.0\ 10^3\ \text{ppm}^{-1}\ \text{min}^{-1}$. The free radical $OH\cdot$ is active at extremely low concentrations through reaction cycles in which $OH\cdot$ is produced and consumed. $OH\cdot$ is produced by photochemical reactions such as

$$HONO + h\nu\ (\lambda < 400\ \text{nm}) \rightarrow OH\cdot + NO \tag{9-23}$$

$$O_3 + h\nu\ (\lambda < 319\ \text{nm}) \rightarrow O_2 + O\cdot \tag{9-24}$$

$$O\cdot + H_2O \rightarrow 2\,OH\cdot \tag{9-25}$$

$$H_2O_2 + h\nu \rightarrow 2\,OH\cdot \tag{9-26}$$

$$NO + HO_2\cdot \rightarrow NO_2 + OH\cdot \qquad (9\text{–}27)$$

etc.

and is terminated at dark by recombination of peroxyl radicals

$$HO_2\cdot + HO_2\cdot \rightarrow H_2O_2 + O_2 \qquad (9\text{–}28)$$

9.4.2 The NO – to – NO_3^- Formation

The formation of atmospheric nitrates is often as important as sulfate formation. We have seen in the previous sections that the primary emissions of NO can be oxidized into NO_2, which forms nitric acid through several mechanisms, such as

$$OH\cdot + NO_2 \rightarrow HNO_3 \qquad (9\text{–}29)$$

and

$$NO_2 + O_3 \rightarrow NO_3 + O_2 \qquad (9\text{–}30)$$

$$NO_3 + HO_2\cdot \rightarrow HNO_3 + O_2 \qquad (9\text{–}31)$$

Then, if NH_3 is present, HNO_3 will generate ammonium nitrate (NH_4NO_3) in condensed or particulate form.

As done before for the SO_2 – to – SO_4^{2-} reaction, NO_2 – to – NO_3^- conversion can be parameterized (SAI, 1984) as a simple function of $OH\cdot$ concentration by

$$-\frac{1}{[NO_2]}\frac{d[NO_2]}{dt} = k_{32}[OH] \qquad (9\text{–}32)$$

where $k_{32} \simeq 1.4\ 10^4\ \text{ppm}^{-1}\ \text{min}^{-1}$.

9.4.3 Aerosol Models

The simulation of the dynamics of multicomponent atmospheric aerosols is a formidable problem that includes (Pilinis et al., 1987) new particle formation by homogeneous heteromolecular nucleation, gas–to–particle conversion, coagulation and dry deposition. A spatially–uniform, dynamic multicomponent aerosol

can be characterized by its size-distribution distribution function, whose dynamic behavior is governed by the "general dynamic equation" (Gelbard and Seinfeld, 1979; Seinfeld, 1986). The sectional approximation of this equation uses, instead of a continuous size distribution for each aerosol species, a series of step functions (Warren and Seinfeld, 1985), as follows

$$\frac{\partial c_{ij}}{\partial t} + \nabla \cdot (\bar{\mathbf{u}}\, c_{ij}) = \nabla \cdot (\mathbf{K}\, \nabla c_{ij}) + \left[\frac{\partial c_{ij}}{\partial t}\right]_{\text{cond./evapor.}} + \left[\frac{\partial c_{ij}}{\partial t}\right]_{\text{coag.}} + \left[\frac{\partial c_{ij}}{\partial t}\right]_{\text{sources/sinks}} \tag{9-33}$$

where c_{ij} is the mass concentration of species i in the j-th size section, $\bar{\mathbf{u}}$ is the average wind field, and $\mathbf{K}$ is the diffusivity tensor. (This equation follows the K-theory described in Chapter 6.)

Equation 9-33 is a general dynamic equation. It can be approximated in three different ways: 1) solving the continuous size distribution numerically; 2) using a step-function approximation and solving numerically (the preferred approach); or, 3) using log-normal distributions and solving numerically. Seigneur et al. (1986) performed a comparative review of these three approaches.

An idealized schematic of the composition of atmospheric aerosols is presented in Figure 9-6. An aerosol model must be able to account for both inorganic and organic constituents. For inorganic aerosols, three models have been developed (Pilinis et al., 1987) to determine the thermodynamic equilibrium of the sulfate-nitrate-chloride-sodium-ammomium-water system, where the following components are possible

- gas phase : NH_3, HCl, HNO_3, H_2O
- liquid phase : H_2O, NH_4^+, SO_4^{2-}, NO_3^-, H^+, Na^+, Cl^-, HSO_4^-, H_2SO_4
- solid phase : Na_2SO_4, $NaHSO_4$, $NaCl$, $NaNO_3$, NH_4Cl, NH_4NO_3, $(NH_4)_2SO_4$, NH_4HSO_4, $(NH_4)_3\,H(SO_4)_2$

These three models account for the rates of transfer of each species between the gas and aerosol phases and, given the sulfate, the HNO_3 and NH_3 concentrations, as well as temperature and relative humidity, are able to determine the equilibrium phase of the system by minimizing the total Gibbs free energy.

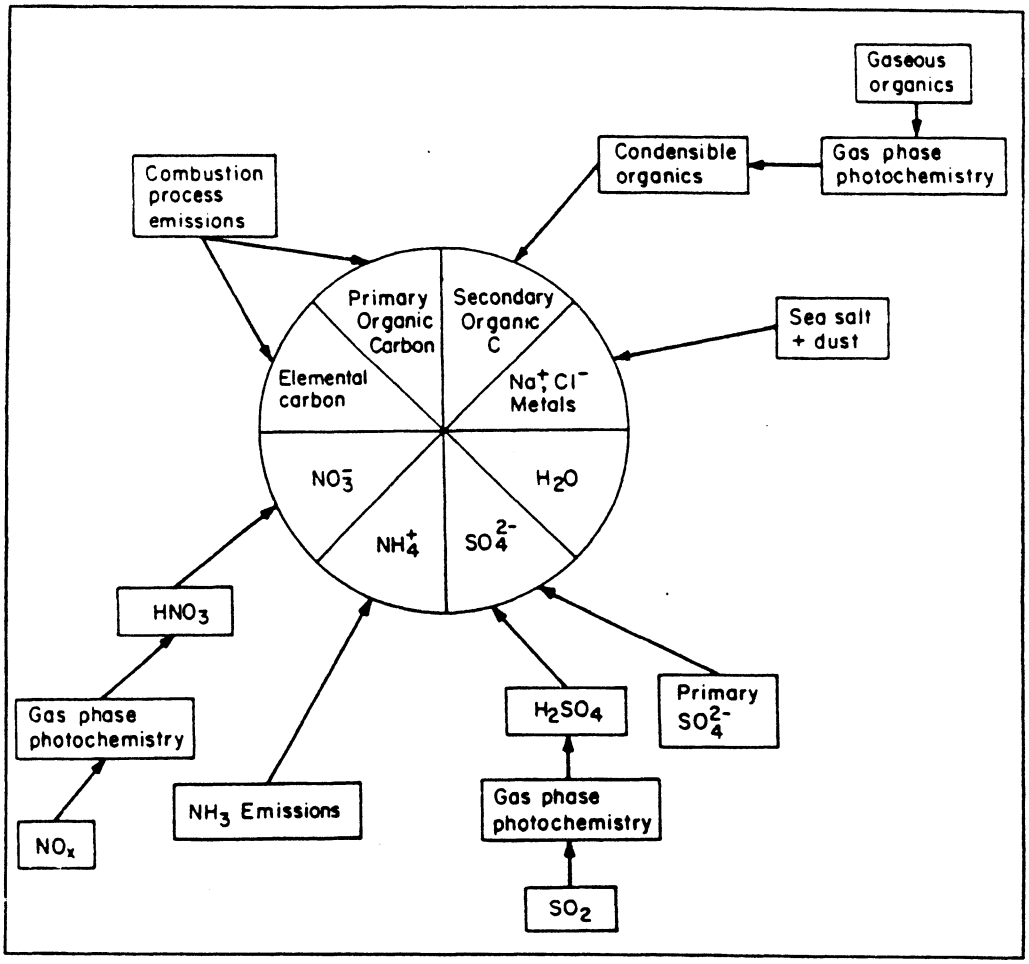

Figure 9–6. Idealized schematic of the composition of atmospheric aerosols. The principal sources and particle formation mechanisms are indicated (from Pilinis and Seinfeld, 1988). [Reprinted with permission from Pergamon Press.]

Organic particulate matter is made of both primary and secondary organic compounds. Primary aerosols result from condensation of various organic species that are the product of gas-phase photooxidation of primary hydrocarbons. The simulation of secondary organic species is difficult and, in spite of several experimental studies, many reaction pathways and physical properties of various condensable species are not well understood.

The Eulerian gas-aerosol model developed by Pilinis and Seinfeld (1988) was applied to simulate air quality in the South Coast Air Basin of California, on a day (30 August 1982) for which 4-h average concentrations data for sulfate,

nitrate, ammonium, chloride, sodium, calcium and magnesium were available. The model, which may require the solution of as many as 224,730 ordinary differential equations, used about 8 CPU hours of a CRAY X-MP for a one-day simulation. Model outputs are encouraging, showing predictions of aerosol concentrations generally within the uncertainty of the measurements. This model, which has provided the first three-dimensional predictions of the concentrations and size distributions of inorganic and organic aerosols in an urban region, shows that water plays an important role (it is more than 50 percent of the aerosol mass at humidities above 80 percent). The major inorganic aerosol species were secondary (sulfates and nitrates), while primary organics were the major organic aerosol species.

The complex photochemical aerosol models discussed above can be used only for episodic situations. Other techniques should be used for long-term simulations. For example, Tesche and McNally (1989) developed the Annual Average Urban Airshed Model (3AM) — a software structure designed to use routine emissions, meteorological and air quality data to predict hourly ozone concentrations over the period of a month or a year (plans for including secondary PM_{10} aerosols and air toxics have also been designed by the authors).

9.5 AIR TOXICS

One of the most important developments in air quality studies and regulation is the growing awareness of the toxicity of airborne chemical species. Specific legislation has identified and classified suspected carcinogenic and mutagens. The assessment of the population risk of exposure to these substances has become a key technical and regulatory issue, at least in the United States.

Air toxics can undergo different chemical reactions and their reactivities are know to vary greatly. Chemical reactions may decrease, with time, the concentrations of certain toxic pollutants. Unfortunately, the opposite is also true, and chemicai reactions can, sometimes, transform a contaminant into an air toxic species.

Seigneur (1987) illustrates the range of chemical behavior of air toxics by discussing the chemistry of four species: chromium (Cr), benzo(a)pyrene (BaP), benzene (C_6H_6) and formaldehyde ($HCHO$).

Chromium, which is emitted as particulate matter, exists in the atmosphere in two stable oxidation states: Cr (III) and Cr (VI). The latter is suspected

to be a carcinogenic compound, while, for the former, no evidence of carcinogenicity is available at the present time. The assessment and quantification of the chemistry patterns *Cr* (III) ⇔ *Cr* (VI) are, therefore, extremely important to assess the potential toxicity of chromium emissions.

The carcinogenicity of benzo(a)pyrene (*BaP*) is well recognized. Its half-life in the atmosphere is highly variable, depending upon its exposure to different species, such as NO_2 and O_3. *BaP* half-life can vary from 35 minutes to several hours, with results much different exposure effects.

Benzene chemistry is relatively simple, since it reacts primarily with $OH\cdot$ and has a lifetime of 15 to 150 hours. Due to the complexity of the urban photochemistry, however, $OH\cdot$ concentrations are often highly uncertain and do not allow precise estimates of benzene reactivity.

Formaldehyde has been shown to be carcinogenic to rats, even though there is no evidence of carcinogenicity in humans. This substance plays a key role both in photochemical smog formation (see Table 9-2) and as an indoor pollutant. It is a good example of toxic pollutants that are also very reactive in the atmosphere.

The four examples above indicate the importance of understanding and correctly simulating the chemistry of air toxic substances. Reliable simulations, tested against the limited data available, can then be used to calculate the population exposure to air toxics and the expected consequences of this exposure (e.g., in terms of risk factors of cancer induction and noncarcinogenic effects, both chronic and acute).

REFERENCES

Ames, J., T.C. Myers, L.E. Reid, D.C. Whitney, S.H. Golding, S.R. Hayes, and S.D. Reynolds (1985a): SAI Airshed Model Operations Manual. Vol. I: User's Manual. U.S. EPA Publication EPA-600/8-85-007a. U.S. Environmental Protection Agency, Research Triangle Park, North Carolina. (NTIS No. PB 85-191567)

Ames, J., S.R. Hayes, T.C. Myers, and D.C. Whitney (1985b): SAI Airshed Model Operations Manuals. Vol. II: Systems Manual. EPA Publication EPA-600/8-85-007b. U.S. Environmental Agency, Research Triangle Park, North Carolina.

Applied Modeling, Inc. (1985): User's guide to the photochemical trajectory model trace. API, Woodland Hills, California.

Atkinson, R., and A.C. Lloyd (1984): Evaluation of kinetic and mechanism data for modeling of photochemical smog. *J. Phys. Chem. Ref. Data*, **13**:315-444.

Baulch, D.L., R.A. Cox, P.J. Crutzen, R.F. Hampson, Jr., F.A. Kerr, J. Troe, and R.P. Watson (1982): Evaluated kinetic and photochemical data for atmospheric chemistry, Supplement 1. CODATA Task Group on Chemical Kinetics, *J. Phys. Chem. Ref. Data*, **11**:327-496.

Carmichael, G.R., L.K. Peters, and T. Kitada (1986): A second generation model for regional-scale transport/chemistry/deposition. *Atmos. Environ.*, **20**:173-188.

Carter, W.P. (1988): Documentation of a gas phase photochemical mechanism for use in airshed modeling, Appendix B. Contract No. A5-122-32. University of California, Statewide Air Pollution Research Center, Riverside, California.

Dodge, M.C. (1977): Combined use of modeling techniques and smog chamber data to derive ozone-precursor relationships. *Proceedings*, International Conference on Photochemical Oxidant Pollution and Its Control, Vol. II, edited by B. Dimitriades, U.S. Environmental Protection Agency Document EPA-600/3-77-001b, pp. 881-889.

Finlayson-Pitts, B.J., and J.N. Pitts, Jr. (1986): *Atmospheric Chemistry: Fundamental and Experimental Techniques*. New York: John Wiley.

Gelbard, F., and J.H. Seinfeld (1979): The general dynamic equation for aerosols—theory and application to aerosol formation and growth. *J. Colloid Interface Sci.*, **69**:363-382.

Gery, M.W., G.Z. Whitten, and J.P. Killus (1987): Development and testing of the CBM-IV for urban and regional testing. U.S. EPA Contract 68-02-4136. Systems Applications, Inc., San Rafael, California.

Gipson, G.L. (1984): User's manual for OZIPM-2: Ozone isopleth plotting with optional mechanisms/Version 2. U.S. Environmental Protection Agency Document EPA-450/4-84-024, Office of Air Quality Planning and Standards, Monitoring and Data Analysis Division, Research Triangle Park, North Carolina.

Kerr, J.A., and J.G. Calvert (1984): Chemical transformations modules for Eulerian acid deposition models, I. The gas-phase chemistry. U.S. Environmental Protection Agency, Research Triangle Park, North Carolina.

Leone, J.A., and J.H. Seinfeld (1984): Updated chemical mechanism for atmospheric photooxidation of toulene. *Int. J. Chem. Kinetics*, **16**:159.

Lurmann, F.W., D.A. Godden, and H.M. Collins (1985): User's guide to the PLMSTAR air quality simulation model. Environmental Research & Technology Document M-2206-100, Newbury Park, California.

McRae, G.J., W.R. Goodin, and J.H. Seinfeld (1982a): Mathematical modeling of photochemical air pollution. Final Report to the California Air Resources Board, Contracts A5-046-87 and A7-187-30.

McRae, G.J., W.R. Goodin, and J.H. Seinfeld (1982b): Development of a second-generation mathematical model for urban air pollution; I. Model formulation. *Atmos. Environ.*, **16**:679.

McRae, G.J., and J.H. Seinfeld (1983): Development of a second generation mathematical model for urban air pollution; II. Evaluation of model problems. *Atmos. Environ.*, **17**:501.

Pilinis, C., J.H. Seinfeld, and C. Seigneur (1987): Mathematical modeling of the dynamics of multicomponent atmospheric aerosols. *Atmos. Environ.*, **21**:943-955.

Pilinis, C., and J.H. Seinfeld (1988): Development and evaluation of an Eulerian photochemical gas-aerosol model. *Atmos. Environ.*, **22**:1985-2001.

Seigneur, C., T.W. Tesche, P.M. Roth, M.-K. Liu (1983): On the treatment of point source emissions in urban air quality modeling. *Atmos. Environ.*, **17**(9):1655-1676.

Seigneur, C., A.B. Hudischewskyj, J.H. Seinfeld, K.T. Whitby, E.R. Whitby, J.R. Brock, and H.M. Barnes (1986): Simulation of aerosol dynamics: A comparative review of mathematical models. *Aerosol Sci. and Tech.*, **5**:205-222.

Seigneur, C. (1987): Computer simulation of air pollution chemistry. *Environ. Software*, **2**:116.

Seinfeld, J.H. (1986): *Atmospheric Chemistry and Physics of Air Pollution*. New York: John Wiley.

Systems Applications, Inc. (1984): Visibility and other air quality benefits of sulfur dioxide emission controls in the eastern United States: Volume I. Systems Applications draft report SYSAPP-84/165, San Rafael, California.

Tesche, T.W., C. Seigneur, W.R. Oliver, and J.L. Haney (1984): Modeling ozone control strategies in Los Angeles. *J. Environ. Eng.*, **110**:208-225.

Tesche, T.W., and D.E. McNalley (1989): A three-dimensional photochemical-aerosol model for episodic and long-term simulation: Formulation and initial application in the Los Angeles Basin. Presented at the annual meeting of the American Chemical Society, Miami Beach, Florida, September.

Warren, D.R., and J.H. Seinfeld (1985): Simulation of aerosol size-distribution evolution in systems with simultaneous nucleation, condensation and coagulation. *Aerosol Sci. & Technol.*, **4**:31-43.

Whitten, G.Z., and H. Hogo (1977): Mathematical modeling of simulated photochemical smog. U.S. Environment Agency Report EPA-600/3-77-011. Research Triangle Park, North Carolina.

Whitten, G.Z., H. Hogo, and J.P. Killus (1980): The carbon-bond mechanism: A condensed kinetic mechanism for photochemical smog. *Environ. Sci. & Technol.*, **14**:690.